

# A chiral quark model for meson electro-production in the region of D-wave resonances

B. Golli<sup>1a</sup> and S. Širca<sup>2b</sup>

<sup>1</sup> Faculty of Education, University of Ljubljana and J. Stefan Institute, 1000 Ljubljana, Slovenia

<sup>2</sup> Faculty of Mathematics and Physics, University of Ljubljana and J. Stefan Institute, 1000 Ljubljana, Slovenia

November 5, 2018

**Abstract.** The meson scattering and electroproduction amplitudes in the D13, D33 and D15 partial waves are calculated in a coupled-channel formalism incorporating quasi-bound quark-model states, extending our previous studies of the P11, P33 and S11 partial waves. The vertices of the baryon-meson interaction including the  $s$ - and  $d$ -wave pions and  $\rho$ -mesons, the  $s$ -wave  $\eta$ -meson, and the  $s$ - and  $p$ -wave  $\sigma$ -mesons are determined in the Cloudy Bag Model, with some changes of the parameters to reproduce the widths of the resonances. The helicity amplitudes and the electroproduction amplitudes exhibit consistent behavior in all channels but tend to be too weak compared to the experiment. We discuss possible origins of this discrepancy which arises also in the constituent quark model calculations.

## 1 Introduction

In our previous research [1–3] we have investigated the  $P$ - and  $S$ -wave nucleon resonances in the intermediate energy region using a coupled-channel formalism which provides an unified treatment of the scattering and the electroproduction processes. The formalism incorporates in a consistent way the quark-model resonance states as excitations of the quark core supplemented by a cloud of mesons. The most important conclusion of these studies was that the main component of the resonance state is indeed the single-particle excitation of the quark core as predicted by the quark model in which a single-quark is excited either to the  $2s$  state (in the case of the  $P$ -wave resonances), or into the  $1p$  state (in the case of the  $S$ -wave). Excitations of the meson cloud may also represent an important component of the excited state. We have found that while the scattering amplitudes can be well reproduced in different models of resonances by a modest readjustment of model parameters, the decisive test of the model is the  $Q^2$ -behavior of the electroproduction amplitudes. By observing the amplitude at lower  $Q^2$  and intermediate  $Q^2$  it may be possible to disentangle the contribution of the pion cloud, which dominates at the periphery, from the contribution of the quark core. In general, we have found that the meson cloud plays an important role, in particular in the EM processes that are sensitive to the long-range behavior of the resonance wave-function. The most evident examples are the dominance of the pion cloud in the quadrupole excitation of the  $\Delta(1232)$  [4] and the zero crossing of the helicity amplitude in the  $N(1440)$  [2].

In the present approach we apply the method to the low-lying  $D$ -wave resonances. Our aim is to check whether the quark core excitation is the principal mechanism for the resonance formation also in this partial wave and, secondly, to study effects of the meson cloud in order to check whether similar effects that were identified in  $S$ - and  $P$ -waves are also presented in the  $D$ -wave resonances. In addition, our approach gives an opportunity to study the two-meson decays as a supplementary method to investigate the underlying resonance dynamics.

Experimentally, helicity amplitudes and electroproduction multipoles have been extracted from the measured quantities (cross-sections and polarization observables) in single- and double-pion electroproduction experiments at Jefferson Lab, Mainz, and Bonn (see [5,6] for a review). In the analysis of single-pion data, unitary isobar models like MAID [7–9] and UIM [10] have been used, as well as dispersion relations approaches [10]; the two-pion channels have been analyzed in the JLab-MSU model [11]. The multipole amplitudes are also obtained in partial-wave analyses (*e.g.* SAID [12,13], Bonn-Gatchina [14], Gießen [15], Zagreb [16], and Kent State [17]), all of which rest on different assumptions and technical details that in many instances render mutually inconsistent results.

The low-lying  $D$ -wave resonances have been explored by systematic studies of photoproduction and pion-induced production of non-strange and strange mesons in chiral unitary approaches [18,19], dynamical coupled-channel approaches like the Jülich 2012 model [20,21], and the model developed by EBAC at JLab [22–25]. In the quark model only helicity amplitudes have been calculated [26–32].

In the next section we briefly review our method. We introduce a more general approach to the treatment of the decay into an unstable intermediate baryon and a me-

<sup>a</sup> e-mail: bojan.golli@ijs.si

<sup>b</sup> e-mail: simon.sirca@fmf.uni-lj.si

son in which the intermediate baryon decays into two or more channels. In sect. 3 the quark structure of the considered resonances is specified and the parameters of the underlying quark model are discussed. In sect. 4 we display the results for the scattering amplitudes in the considered partial wave and present our prediction for the widths and the branching fractions for the  $N(1520)D13$ ,  $N(1700)D13$ ,  $N(1675)D15$  and  $\Delta(1700)D33$  resonances. In sect. 5 we discuss the results for the transverse helicity amplitudes  $A_{1/2}$  and  $A_{3/2}$  for the  $N(1520)$ ,  $N(1675)$  and  $\Delta(1700)$  resonances. In sect. 6 we review the results for pion photoproduction, separately for the  $E_{2-}$  and  $M_{2-}$  ( $M_{2+}$ ) amplitudes. The last section contains some concluding remarks.

## 2 Basics of the coupled-channel approach

In our previous work [1] we have developed a method in which the quasi-bound quark-model states are incorporated in the channel states obeying proper asymptotic behavior. We have shown that such states can be cast in the form

$$|\Psi_{JI}^{MB}\rangle = \mathcal{N}_{MB} \left\{ [a^\dagger(k_M)|\tilde{\Psi}_B]^{JI} + \sum_{\mathcal{R}} c_{\mathcal{R}}^{MB} |\Phi_{\mathcal{R}}\rangle + \sum_{M'B'} \int \frac{dk}{\omega_k + E_{B'}(k) - W} [a^\dagger(k)|\tilde{\Psi}_{B'}]^{JI} \right\}, \quad (1)$$

where the first term represents the free meson ( $\pi$ ,  $\eta$ ,  $\rho$ ,  $K$ , ...) and the baryon ( $N$ ,  $\Delta$ ,  $\Lambda$ , ...) and defines the channel, the next term is the sum over *bare* three-quark states  $\Phi_{\mathcal{R}}$  involving different excitations of the quark core, while the third term describes meson clouds around different isobars. Here  $W$  is the invariant energy,  $J$  and  $I$  are the angular momentum and isospin of the meson-baryon system,  $\omega_M$  and  $k_M$  are the energy and momentum of the incoming (outgoing) meson,  $\tilde{\Psi}_B$  is a properly normalized baryon state (see appendix A) and  $E_B$  is its energy. The normalization factor is  $\mathcal{N}_{MB} = \sqrt{\omega_M E_B / (k_M W)}$ . The integration over meson momenta is defined in the principal value sense. Considering chiral quark models in which mesons couple linearly to the quark core, the  $K$  matrix element between the meson-baryon channels (labeled by  $MB$  and  $M'B'$ , respectively) can be written in the form

$$K_{M'B' MB}^{JI} = -\pi \mathcal{N}_{M'B'} \langle \Psi_{JI}^{MB} || V_{M'}(k) || \tilde{\Psi}_{B'} \rangle, \quad (2)$$

where  $V_{M'}(k)$  stands for the quark-meson vertex of the underlying quark model and  $\tilde{\Psi}_{B'}$  is the baryon state in the  $M'B'$  channel.

The meson amplitudes  $\chi^{M'B' MB}(k, k_M)$  are proportional to the (half) off-shell matrix elements of the  $K$  matrix and are determined by solving an equation of the Lippmann-Schwinger type. The resulting matrix elements

of the  $K$  matrix take the form

$$K_{M'B' MB}(k, k_M) = - \sum_{\mathcal{R}} \frac{\mathcal{V}_{BR}^M(k_M) \mathcal{V}_{B'\mathcal{R}}^{M'}(k)}{Z_{\mathcal{R}}(W)(W - W_{\mathcal{R}})} + K_{M'B' MB}^{\text{bkg}}(k, k_M), \quad (3)$$

where the first term represents the contribution of various resonances, while  $K_{M'B' MB}^{\text{bkg}}(k, k_M)$  originates in the non-resonant background processes. Here  $\mathcal{V}_{BR}^M$  is the dressed matrix element of the quark-meson interaction between the resonance state and the baryon state in the channel  $MB$ , and  $Z_{\mathcal{R}}$  is the wave-function normalization. The physical resonance state  $\mathcal{R}$  is a superposition of the dressed states built around the bare three-quark states  $\Phi_{\mathcal{R}'}$ . The  $T$  matrix is finally obtained by solving the Heitler equation

$$T_{MB M'B'} = K_{MB M'B'} + i \sum_{M''B''} T_{MB M''B''} K_{M''B'' M'B'}. \quad (4)$$

In our approach we make the usual assumption that the two-pion decay proceeds either through an unstable meson ( $\rho$ -meson,  $\sigma$ -meson, ...) or through a baryon resonance ( $\Delta(1232)$ ,  $N^*(1440)$ , ...). In such a case, the channel depends either on the invariant mass  $M_B$  of the  $M''B''$  subsystem into which the resonance decays, or the invariant mass of the mesons (normally two pions) of the outgoing unstable meson ( $\sigma$  or  $\rho$ ). The unstable-baryon state is normalized as  $\langle \tilde{\Psi}_B(M'_B) | \tilde{\Psi}_B(M_B) \rangle = \delta(M'_B - M_B)$ , where  $M_B$  is the invariant mass of the meson-baryon subsystem. In such cases, the Heitler equation implies also the summation (integration) over the invariant masses of either the baryon-meson or the two-mesons subsystems. The equation can be simplified by noting that close to the resonance the dependence on the invariant mass can be expressed in terms of a weight function corresponding to a specific decay of the resonance. Since in this work we consider the processes at higher energies which involve a decay of the intermediate resonance into two or more channels — a situation not treated in our previous work — we give details of the construction of the orthonormal basis states  $\tilde{\Psi}_B(M_B)$  and the corresponding weight functions in appendix A.

Considering meson electroproduction, the  $T$  matrix for  $\gamma^* N \rightarrow MB$  satisfies

$$T_{MB \gamma N} = K_{MB \gamma N} + i \sum_{M'B'} T_{MB M'B'} K_{M'B' \gamma N}. \quad (5)$$

In the vicinity of a resonance ( $\mathcal{R}$ ) we split the  $K$  matrix into the “resonant” part and the background which includes also all possible other resonances in the considered partial wave:

$$K_{MB \gamma N} = - \frac{\mathcal{V}_{BR}^M \mathcal{V}_{NR}^\gamma}{Z_{\mathcal{R}}(W)(W - W_{\mathcal{R}})} - \sum_{\mathcal{R}' \neq \mathcal{R}} \frac{\mathcal{V}_{BR'}^M \mathcal{V}_{NR'}^\gamma}{Z_{\mathcal{R}'}(W)(W - W_{\mathcal{R}'})} + B_{MB \gamma N}^{\text{bkg}}. \quad (6)$$

From (3) it follows that the first term can be written in the form

$$\frac{\mathcal{V}_{BR}^M \mathcal{V}_{NR}^\gamma}{Z_{\mathcal{R}}(W)(W - W_{\mathcal{R}})} = \left( K_{MB\pi N} - K_{MB\pi N}^{\text{bkg}} \right) \frac{\mathcal{V}_{NR}^\gamma}{\mathcal{V}_{NR}^\pi} \quad (7)$$

so that (5) takes the form

$$\begin{aligned} T_{MB\gamma N} &= \frac{\mathcal{V}_{NR}^\gamma}{\mathcal{V}_{NR}^\pi} T_{MB\pi N} + T_{MB\pi N}^{\text{bkg}} \\ &\equiv T_{MB\gamma N}^{\text{res}} + T_{MB\gamma N}^{\text{bkg}}, \end{aligned} \quad (8)$$

which means that the  $T$  matrix for electroproduction can be split into the resonant part and the background part; the latter is the solution of the Heitler equation with the ‘‘background’’  $K$  matrix defined as

$$\begin{aligned} K_{MB\gamma N}^{\text{bkg}} &= -K_{MB\pi N}^{\text{bkg}} \frac{\mathcal{V}_{NR}^\gamma}{\mathcal{V}_{NR}^\pi} \\ &\quad - \sum_{\mathcal{R}' \neq \mathcal{R}} \frac{\mathcal{V}_{BR'}^M \mathcal{V}_{NR'}^\gamma}{Z_{\mathcal{R}'}(W)(W - W_{\mathcal{R}'})} + B_{MB\gamma N}^{\text{bkg}}. \end{aligned}$$

Note that  $\mathcal{V}_{NR}^\gamma(k_\gamma)$  is proportional to the helicity amplitudes, while the strong amplitude  $\mathcal{V}_{BR}^M(k_M)$  to  $\zeta\sqrt{T_{MB}}$ , where  $\zeta$  is the sign of the meson decay amplitude.

### 3 The D-wave resonances in the quark model

In the quark model, the negative parity  $D$ -wave resonances are described by a single-quark  $p$ -wave ( $l = 1$ ) orbital excitation. The two D13 (flavor octet,  $J = \frac{3}{2}$ ) resonances are superpositions of the spin doublet ( $S = \frac{1}{2}$ ) and quadruplet ( $S = \frac{3}{2}$ ) configurations [33]. We use the  $j$ - $j$  coupling scheme [34] in which the resonances take the following forms:

$$\begin{aligned} N(1520) &= -\sin\vartheta_d |^4\mathbf{8}_{3/2}\rangle + \cos\vartheta_d |^2\mathbf{8}_{3/2}\rangle \\ &= c_S^l |(1s)^2 1p_{3/2}\rangle_{MS} + c_A^l |(1s)^2 1p_{3/2}\rangle_{MA} + c_P^l |(1s)^2 1p_{1/2}\rangle, \end{aligned} \quad (9)$$

$$\begin{aligned} N(1700) &= \cos\vartheta_d |^4\mathbf{8}_{3/2}\rangle + \sin\vartheta_d |^2\mathbf{8}_{3/2}\rangle \\ &= c_S^u |(1s)^2 1p_{3/2}\rangle_{MS} + c_A^u |(1s)^2 1p_{3/2}\rangle_{MA} + c_P^u |(1s)^2 1p_{1/2}\rangle. \end{aligned} \quad (10)$$

Here  $1p_{1/2}$  and  $1p_{3/2}$  denote the single-quark states with  $j = \frac{1}{2}$  and  $j = \frac{3}{2}$ , respectively, and  $MS$  and  $MA$  denote the mixed symmetric and the mixed antisymmetric spatial representation. The coefficients are given as

$$\begin{aligned} c_S &= \frac{2}{3} \begin{Bmatrix} \sin\vartheta_d \\ -\cos\vartheta_d \end{Bmatrix} + \sqrt{\frac{5}{18}} \begin{Bmatrix} \cos\vartheta_d \\ \sin\vartheta_d \end{Bmatrix}, \\ c_A &= -\frac{\sqrt{2}}{2} \begin{Bmatrix} \cos\vartheta_d \\ \sin\vartheta_d \end{Bmatrix}, \\ c_P &= \frac{\sqrt{5}}{3} \begin{Bmatrix} -\sin\vartheta_d \\ \cos\vartheta_d \end{Bmatrix} + \frac{\sqrt{2}}{3} \begin{Bmatrix} \cos\vartheta_d \\ \sin\vartheta_d \end{Bmatrix}, \end{aligned} \quad (11)$$

where the upper values in  $\{\}$  refer to the  $N(1520)$  resonance. The constituent quark model calculations (see *e.g.* [33]) as well as the calculation in the MIT bag model with hyperfine interaction [34,35] predict that the  $^4\mathbf{8}$  configuration is some 150 MeV higher than the  $^2\mathbf{8}$ , suggesting a small value of the mixing angle  $\vartheta_d$ . The small value agrees with the quark-model analysis of the  $\pi N$  decay of the resonances (see *e.g.* [36]) which predicts a nearly negligible decay amplitude of the  $N(1700)$  into the  $\pi N$  channel. Let us note that in the dynamical coupled-channel approaches [20,37] the  $N(1700)$  resonance appears to be dynamically generated, with strong couplings to  $\rho N$  and  $K^* \Lambda$  channels.

The D33 resonance (flavor decuplet) has  $S = \frac{1}{2}$ , while the D15 resonance (octet,  $J = \frac{5}{2}$ ) has  $S = \frac{3}{2}$ , thus

$$\begin{aligned} \Delta(1700)D33 &= |^2\mathbf{10}_{3/2}\rangle \\ &= \frac{\sqrt{5}}{3} |(1s)^2 1p_{3/2}\rangle - \frac{2}{3} |(1s)^2 1p_{1/2}\rangle, \end{aligned} \quad (12)$$

$$N(1675)D15 = |^4\mathbf{8}_{5/2}\rangle = |(1s)^2 1p_{3/2}\rangle. \quad (13)$$

We shall not consider the D35 partial wave since the experimental data in this case are too scarce.

The underlying chiral quark model in our calculations in the P11, P33 and S11 partial waves has been the Cloudy Bag Model [38]. In these studies we kept its parameters fixed to the popular values used in the calculations of nucleon properties, *i.e.* the bag radius  $R = 0.83$  fm, which determines the range of the quark-pion interaction corresponding to the cut-off  $\Lambda \approx 550$  MeV/c, and  $f_\pi = 76$  MeV, which reproduces the experimental value of the  $\pi NN$  coupling constant.

The  $l = 2$  pions couple only to  $j = 3/2$  quarks; the corresponding interaction in the Cloudy Bag Model takes the form

$$\begin{aligned} V_{2mt}^\pi(k) &= \frac{1}{2f_\pi} \sqrt{\frac{\omega_{p_{3/2}}\omega_s}{(\omega_{p_{3/2}} - 2)(\omega_s - 1)}} \frac{\sqrt{2}}{2\pi} \frac{k^2}{\sqrt{\omega_k}} \frac{j_2(kR)}{kR} \\ &\quad \times \sum_{i=1}^3 \tau_t(i) \Sigma_{2m}^{[\frac{1}{2}\frac{3}{2}]}(i), \end{aligned} \quad (14)$$

where  $\omega_s = 2.043$ ,  $\omega_{p_{3/2}} = 3.204$ , and

$$\Sigma_{2m}^{[\frac{1}{2}\frac{3}{2}]} = \sum_{m_s m_j} C_{\frac{3}{2}m_j 2m}^{\frac{1}{2}m_s} |sm_s\rangle \langle p_{3/2}m_j|.$$

In our previous work [3] we have introduced the quark-meson coupling of other members of the SU(3) meson octet, as well as the coupling of the  $\sigma$ - and  $\rho$ -mesons. In the formulas given for the  $\rho$ -quark couplings we have considered only the mesons with transverse polarization, which is justified in the case of positive-parity resonances. A more complete treatment including the construction of  $\rho N$  channels with good spin of the  $\rho N$  system along with the discussion on the  $\sigma$ -quark coupling is given in appendix B.

Assuming SU(3) flavor symmetry all coupling constants of the meson octet are fixed by the value of the  $\pi NN$  coupling constant. The  $\sigma$  and  $\rho$  couplings are free parameters

in principle. Since the results turn out to depend only weakly on these values, and because the data for the corresponding channels are rather uncertain, we assume the same value for the  $\sigma$  coupling as for the one used in the P11 partial wave, while for the  $\rho$ -meson we assume simply  $f_\rho = f_\pi$ .

In order to reproduce the decay widths, as described in the following section, we had to increase the quark-model values for the  $d$ -wave quark-meson couplings and either increase or decrease the  $s$ -wave couplings, while preserving the  $p$ -wave couplings. We note that the wave-function and vertex renormalization through meson loops does not solve the problem of the widths as it has been the case in the Delta(1232) and the N(1440) [1]. In fact, there is a tendency that they even diminish with respect to their bare values by 10 % to 20 %. The  $p$ -wave couplings are not necessarily the bare values; e.g., the  $\pi N\Delta$  coupling is the dressed one, as determined in our calculation in the P33 case.

We use a single renormalization factor for all  $d$ -wave couplings and another one for all  $s$ -wave couplings in the given partial wave (with one exception in the D15 wave), thus keeping the number of free parameters small. The fact that only a single factor is needed would follow naturally if the behavior of the quark wave-functions were improved.

The predictive power of the quark model can be judged upon two considerations: by assessing the corrections needed to reproduce the pion-nucleon scattering amplitudes, and by comparing the helicity or total photo-production amplitudes to data. It is crucial to note that the latter receives input from the former, hence the strong part needs to be controlled well before being able to assess the quality of the electromagnetic contribution.

In addition to the renormalization factors, the adjustable parameters are the positions of the  $K$ -matrix poles of the resonances. Typical differences between bare and pole masses are: 200 MeV (for D13), 240 MeV (D15), and 500 MeV (D33). These values are generally smaller compared to those in the calculations in dynamical models (see e.g. [20]) as a consequence of the smaller cut-off (i.e. larger bag radius) used in our calculation.

## 4 The scattering amplitudes

The behavior of the scattering amplitudes in the D13 partial wave is governed by a subtle interplay of the elastic and — primarily — the  $s$ -wave  $\pi\Delta$  channel. As we have mentioned in the previous section, the lower  $N(1520)$  resonance is predominantly the  ${}^2\mathbf{8}$  configuration. It is strongly coupled to the  $\pi N$  channel and moderately to the  $s$ -wave  $\pi\Delta$  channel. The upper  $N(1700)$  resonance is then mainly the  ${}^4\mathbf{8}$  configuration; its quark model coupling to the  $\pi N$  channel is a factor of  $3\sqrt{5}$  weaker than in the  ${}^2\mathbf{8}$  configuration, but stronger in the case of the  $\pi\Delta$  channel. The corresponding ratio in the  $\pi\Delta$  channel is  $\sqrt{5/2}$  for the  $s$ -wave and  $-\sqrt{8/5}$  for the  $d$ -wave pions. As already noted by Hey et al. [36] this explains qualitatively the observed behavior of the decay amplitudes.

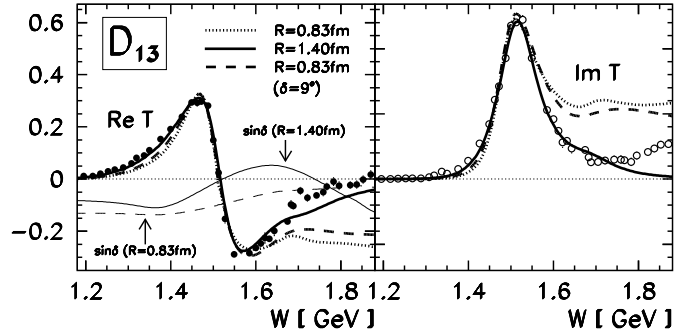


**Fig. 1.** The real and imaginary part of the elastic scattering  $T$  matrix for the D13 partial wave for three choices of parameters: bag radius  $R = 0.83$  fm (thick dotted line),  $R = 1.40$  fm (thick full line), both with  $W$ -dependent  $\vartheta_\delta$ , and  $R = 0.83$  fm with fixed  $\vartheta_\delta = 9^\circ$  (thick dashed line). The data points are from the SAID  $\pi N \rightarrow \pi N$  partial-wave analysis [12,13]. Also shown is the sine of the mixing angle between spin  $\frac{1}{2}$  and  $\frac{3}{2}$  configurations defined in (9) and (10).

In our coupled-channel calculation we have included in addition to the elastic and the  $s$ - and  $d$ -wave  $\pi\Delta$  channels also the  $p$ -wave  $\sigma N$  channel, the  $d$ -wave  $\pi N(1440)$  and  $\eta N$  channels, as well as the  $s$ - and  $d$ -wave  $\rho N$  channels. For our standard choice of the model parameters discussed in the previous section the calculated elastic amplitude turns out to be too weak, while the  $s$ -wave  $\pi\Delta$  decay amplitude is overestimated. This effect is further enhanced if we allow for the mixing of the two resonances through  $s$ - and  $d$ -wave pion loops with the intermediate  $\Delta$  and the nucleon. The elastic width of the lower resonance is reproduced only if we increase the  $d$ -wave pion coupling to the  $\pi N$  channel by 50 % and reduce the  $s$ -wave coupling to the  $\pi\Delta$  channel by almost 40 %.

The agreement with the data improves considerably if we increase the bag radius to 1.4 fm. If we increase simultaneously the couplings of the  $d$ -wave pions by 35 % and reduce the  $s$ -wave  $\pi\Delta$  coupling by 15 % with respect to their quark-model values, we obtain an almost perfect agreement with experiment, as shown in fig. 1. As we discuss in the next section, the results for the magnetic quadrupole excitation amplitude also favor larger bag radii, however, the dominant electric dipole excitation diminishes considerably in such a case. The effect on the choice of the mixing angle  $\vartheta_d$  introduced in (9) is shown for a fixed value  $\vartheta_d = 9^\circ$  (close to the value suggested by [36] and [33]) and the value calculated through the pion loops which introduces the energy dependent mixing.

We therefore keep the radius at  $R = 1$  fm which still yields consistent values for the ground-state properties. At this value, the  $d$ -wave coupling strength has to be increased by 43 % with respect to its quark-model value in order to reproduce the experimental width of the resonance,  $\Gamma = 115$  MeV. The inelastic channels are still dominated by the  $s$ -wave  $\pi\Delta$  channel (with the  $s$ -wave coupling reduced to 58 % of its quark-model value) as seen in table 1 and fig. 2. As mentioned in the previous section, we use  $\tilde{f}_\rho = f_\pi$  for the parameter appearing in

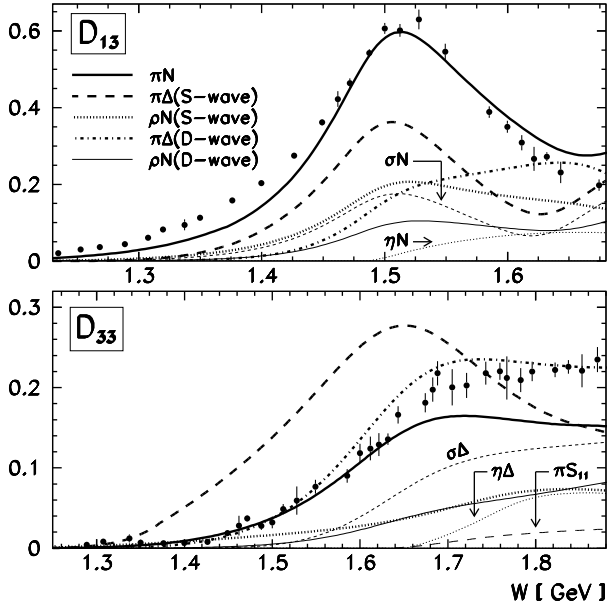


**Fig. 2.** The absolute values  $|T_{MB \pi N}|$  of the amplitudes for the elastic and the dominant inelastic channels in the D13 partial wave (top panel) and in the D33 partial wave (bottom panel). The  $\sigma$  meson and the pion in  $\pi S_{11}$  channel are in the relative  $p$ -wave and the  $\eta$  meson in the  $s$ -wave.

the  $\rho$ -quark coupling (see appendix B). This is somewhat stronger with respect to the value that would follow from the conventional values for the  $\rho NN$  coupling; still the branching fraction for the  $s$ -wave  $\rho N$  channel is below the PDG value. The branching fraction for the  $\eta N$  channel at 1520 MeV (not displayed in table 1) is 0.10 %, close to the value found in [39, 13, 20] but smaller compared to that in [15].

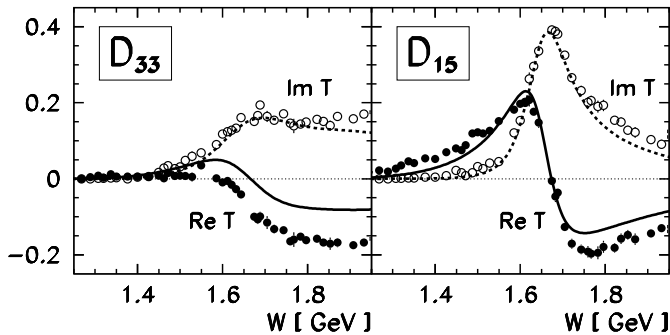


**Fig. 3.** The real and imaginary part of the elastic scattering  $T$  matrix for the D33 (left) and D15 (right) partial wave. The data points are the same as in fig. 1.

The scattering amplitudes in the D33 partial wave are well reproduced for our standard choice of the bag radius ( $R = 0.83$  fm), provided the  $d$ -wave pion coupling strength is multiplied by a factor 2.4 which gives the total width of 288 MeV (fig. 3). In order to be able to re-

produce the almost flat behavior of the elastic amplitude above the resonance we have included up to 13 inelastic channels: the  $s$ - and  $d$ -wave  $\pi\Delta$  and  $\rho N$  channels, the  $d$ -wave  $\pi N(1440)$  channel, the  $p$ -wave  $\pi N(1535) \rightarrow \pi\pi N$ ,  $\pi N(1535) \rightarrow \pi\eta N$ ,  $\pi N(1650)$ ,  $\sigma\Delta$  and  $\eta\Delta$  channels, and the  $s$ -wave  $\pi\Delta(1600)$  and  $\sigma\Delta(1700)$  channels. The results for the major contributions are presented in table 1 and in fig. 2. Since the width and the branching fractions are evaluated at the  $K$ -matrix pole ( $W = 1680$  MeV) which is relatively low compared to the threshold, some of the interesting channels, such as the  $\eta\pi N$  channel, are not included in the table. In fig. 2 we notice that the contribution of the  $\eta\Delta$  channel becomes sizable only above 1700 MeV and remains stronger compared to the competitive process in which the  $\eta\pi N$  final state is reached through the  $N(1535)$  intermediate state.

The resonant contribution to  $\pi N \rightarrow \rho N$  turns out to be quite small due to a strong cancellation between the  $\rho$  couplings to  $p_{j=1/2}$  and  $p_{j=3/2}$  quarks. The relatively strong amplitude in fig. 2 stems from the background  $u$ -channel process involving predominantly the D13 intermediate state.

Res.	$\pi N$	$\pi\Delta$ (S)	$\pi\Delta$ (D)	$\rho N$	$\sigma$
$N(1520)$	59 %	23 %	5 %	7 % (S)	5 %
PDG	55–65 %	10–20 %	10–15 %	$9 \pm 1$ %	$< 8$ %
$N(1700)$	11 %	35 %	26 %	1 % (S)	25 %
PDG	$12 \pm 5$ %	10–90 %	$< 20$ %	$7 \pm 1$ %	
$\Delta(1700)$	15 %	50 %	29 %	4 % (S)	4 %
PDG	10–20 %	25–50 %	5–15 %	5–20 %	
$N(1675)$	39 %	-	58 %	2 % (D)	-
PDG	35–45 %	-	$50 \pm 15$ %	$1 \pm 1$ %	-

**Table 1.** The branching fractions for  $N(1520)D_{13}$ ,  $N(1700)D_{13}$ ,  $\Delta(1700)D_{33}$  and  $N(1675)D_{15}$ . For the first three resonances only the  $s$ -wave  $\rho N$  values are compared;  $\sigma$  denotes the  $\sigma N$  channel for the D13 resonances and  $\sigma\Delta$  for the D33 case. The PDG values are from [40].

The scattering amplitudes in the D15 partial waves are dominated by the elastic and the  $d$ -wave  $\pi\Delta$  channel (fig. 3 (right) and 4 (left)). We use  $R = 1$  fm for the bag radius. Similarly as in the case of the D33 partial wave, the  $\pi N$  coupling has to be increased by a factor of 2.25, and the  $\pi\Delta$ ,  $\eta N$  and  $\rho N$  couplings by a factor of 1.45 compared to their quark-model values in order to reproduce the experimental width of 150 MeV and the branching fractions (table 1). (The branching fraction for the  $\eta N$  channel is 1.8 %.) In the present model the quarks are excited only to the  $p$ -state, so they do not couple to the  $\sigma$ -meson; the relatively large fraction of the  $\sigma N$  decay seen in the experiment may indicate that the excitation to the  $f$ -state is important.

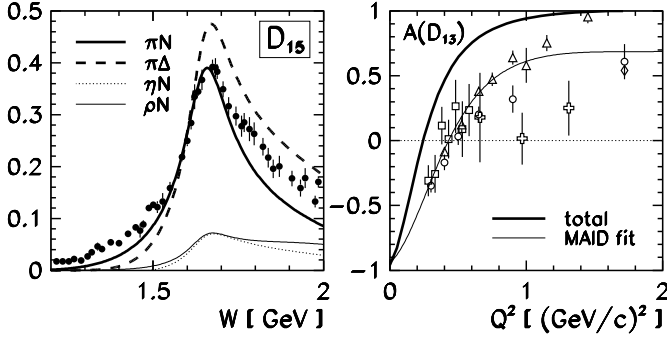


**Fig. 4.** The absolute values  $|T_{MB\pi N}|$  of the scattering amplitudes in the D15 partial wave (left) and the helicity asymmetry  $A = (A_{1/2}^2 - A_{3/2}^2)/(A_{1/2}^2 + A_{3/2}^2)$  for the  $N(1520)D13$  (right).

## 5 The helicity amplitudes for the $D$ -wave resonances.

The resonant part of the electroproduction amplitude, proportional to  $M_{MB\gamma N}^{\text{res}}$  in eq. (8), reads:

$$\mathcal{M}_{MB\gamma N}^{\text{res}} = \sqrt{\frac{\omega_\gamma E_N^\gamma}{\omega_\pi E_N} \frac{\xi}{\pi \mathcal{V}_{N\mathcal{R}}}} \langle \widehat{\Psi}_{\mathcal{R}} | V_\gamma | \Psi_N \rangle T_{MB\pi N},$$

where  $V_\gamma$  is the interaction of the photon with the electromagnetic current, which contains quark and pion contributions, and  $\xi$  is the spin-isospin factor depending on the considered multipole and the spin and isospin of the outgoing hadrons. The matrix element  $\langle \widehat{\Psi}_{\mathcal{R}} | V_\gamma | \Psi_N \rangle$  is the helicity amplitude. The resonance state  $\widehat{\Psi}_{\mathcal{R}}$  is extracted from the components in the second and the third term in (1) that are proportional to the resonance pole  $(W - W_{\mathcal{R}})^{-1}$ ; it involves the bare-quark core and the meson cloud:

$$|\widehat{\Psi}_{\mathcal{R}}\rangle = Z_{\mathcal{R}}^{-\frac{1}{2}} \left[ |\Phi_{\mathcal{R}}\rangle - \sum_{MB} \int \frac{dk}{\omega_k + E_B - W} \frac{\mathcal{V}_{BR}^M(k)}{E_B - W} [a^\dagger(k) |\widetilde{\Psi}_B\rangle]^{JI} \right]. \quad (15)$$

Note that the integration is meant in the principal-value sense, hence the helicity amplitudes are real. In our model the transverse helicity amplitudes are linear combinations of the electric dipole and the magnetic quadrupole amplitudes, see *e.g.* [7]. The latter involve only the  $1p_{3/2}$  quark state and no  $1p_{1/2}$ .

In general, the amplitudes for the  $D$ -wave resonances presented in figs. 5 and 6 are underestimated with respect to the amplitudes extracted from experiments in various analyses. This is a similar situation as in the case of the  $D$ -wave scattering amplitudes and may again indicate that the description of the peripheral part of the resonance wave-function is inadequate. However, such a conclusion holds also for calculations in other quark models; the constituent quark model [29,31,32] predicts a very similar behavior as our model for the helicity amplitudes of the resonances in the D13, D33 and D15 partial wave. On the other hand, the helicity asymmetry for the  $N(1520)$  (fig. 4

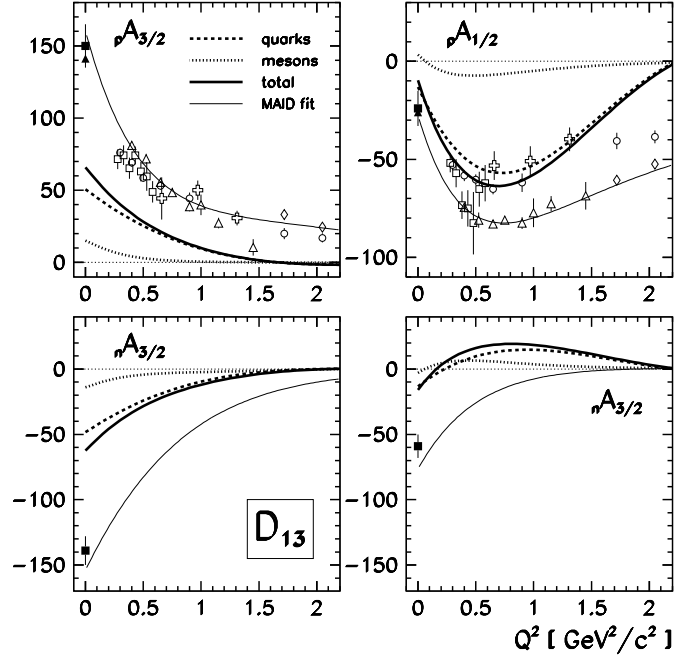


**Fig. 5.** Helicity amplitudes for electroexcitation of the D13 resonance. Top panels: proton target. Bottom panels: neutron target. The data points are: the PDG values [40] (filled squares), pion photoproduction data from CLAS [41] (filled triangles), average of dispersion-relation analyses and unitary-isobar model of [10] (empty circles), JLab-MSU analysis of two-pion electroproduction at CLAS [11] (empty squares), MAID2007 analysis [7] based on cross-sections of refs. [42,43] (empty triangles), MAID2008 reanalysis [8] based on cross-sections of ref. [44] (empty diamonds) and JLab two-pion analysis [6] (empty crosses).

(right)) confirms the changeover to the helicity-1/2 dominance at higher  $Q^2$ , and follows the general trend in the quark model first predicted by [26].

In our calculation, the effect of the meson cloud, *i.e.* processes in which the photon couples directly to the pion as well as the vertex corrections, are generally relatively strong. In the constituent quark model, however, the effects of the pion cloud have not been taken into account in the considered partial waves; but as shown in [45,46] for the P33 partial-wave, these effects can be strong in the constituent quark models too. We can therefore conjecture that using a more elaborate model to describe the quark core and the meson cloud might eventually bring the calculated amplitudes in agreement with the experiment — considering also the large scatter of experimental values. The meson cloud contribution to the D13 helicity amplitudes calculated in the Dynamical Coupled Channel Approach [23] shows even a stronger contribution than in the present calculation, which could be attributed to the inclusion of the  $\gamma\rho\pi$  and  $\gamma\omega\pi$  vertices that are absent in our approach. Similarly, the importance of the meson-cloud contribution found in our approach in the case of the  $\Delta(1700)D33$  resonance is in line with the chiral uni-

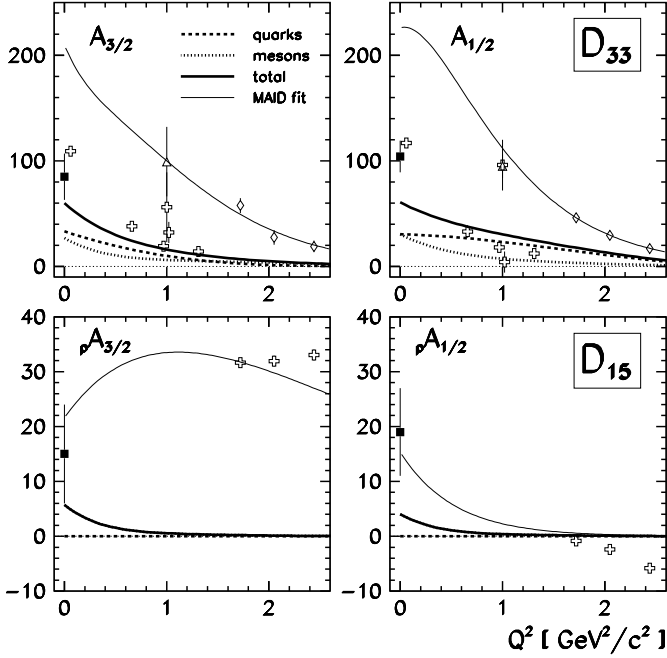


**Fig. 6.** Helicity amplitudes for electroexcitation of the D33 (top panels) and D15 resonance (bottom panels). Notation for data points as in fig. 5.

tary approach [18], in which the entire radiative width comes from the meson cloud.

In the case of the  $N(1675)D_{15}$  resonance we observe a strong deviation of the calculated  $A_{3/2}$  and  $A_{1/2}$  amplitudes at larger  $Q^2$  compared to the experiment [9]. As we have mentioned, in the present approach we assume only  $p$ -wave excitation of the quark core and the  $s$ - and  $d$ -wave excitation of the meson cloud, in which case only the magnetic quadrupole excitation contributes and the helicity amplitudes are simply related by  $A_{3/2} = \sqrt{2}A_{1/2}$ . Furthermore, the quark contribution to the isoscalar proton amplitude cancels the isovector one, which is the main reason that the amplitudes almost vanish at larger  $Q^2$ . In order to reproduce the behavior of the amplitudes as extracted from the experiment, a rather strong contribution of the  $f$ -wave quark excitation has to be assumed; note that the importance of the  $f$ -wave excitation has been mentioned already in the previous section as a possible explanation of the relatively large decay probability into the  $\sigma N$  channel.

## 6 The photoproduction amplitudes

The photoproduction amplitudes consist of the resonant and the background contribution. In our approach, the background term originates from the pion pole which governs the amplitudes at low energies, the contribution from the  $u$ -channel processes and, in the case of the D13 partial wave, from the contribution of the upper resonance. In the vicinity of a resonance, the amplitudes are dominated

by the resonant contribution which turn out to be significantly underestimated, as could be anticipated from our results for the helicity amplitudes in the previous section.

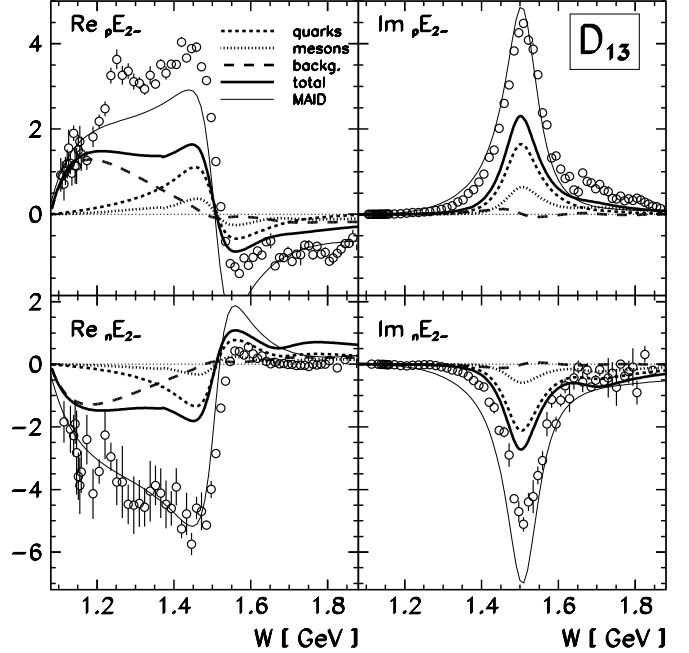


**Fig. 7.** The real and imaginary parts of the  $E_{2-}$  electroproduction amplitude (in units of  $10^{-3}/m_{\pi}$ ) in the D13 partial wave, for the proton (top panels) and neutron target (bottom panels). The curves corresponding to our calculation are: resonance quark core (dashed) and meson cloud (dotted), background (long-dashed), and total (thick full lines). The experimental points are taken from the SAID analysis [13]. The MAID fit is shown by thin full lines.

Regarding the magnetic quadrupole contribution, the agreement with the experiment can be considerably improved by increasing the bag radius to  $R \approx 1.4$  fm. However, the electric dipole contribution becomes even smaller in such a case; also, the amplitude drops to zero too quickly at larger  $Q^2$ .

Although the strength of all amplitudes is underestimated, the amplitudes do show a consistent behavior for all multipoles and for all partial waves. In particular, our results for the  $E_{2-}$  amplitude in the D13 partial wave agree with the observation that the amplitudes for the neutron target are slightly stronger than those for the proton, while the  $M_{2-}$  amplitude is correctly predicted to almost vanish in the neutron case.

In the D33 partial wave we stress the important effects of the resonance meson cloud which accounts for almost half of the resonant contribution, bringing the  $E_{2-}$  amplitude close to the experiment; in the case of  $M_{2-}$  this contribution is, however, still too weak and indicates an inadequate description of the resonance periphery.

The effect of the meson cloud is not so pronounced in the D15 partial wave; it represents, however, the sole con-

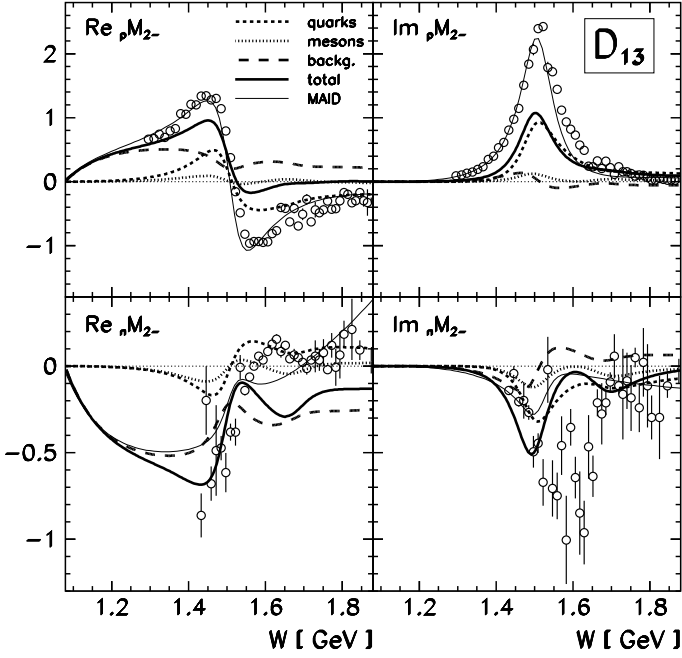


Fig. 8. The real and imaginary parts of the  $M_{2-}$  electroproduction amplitude for the D13 partial wave. Notation as in fig. 7.

tribution in the proton case, since the isoscalar and the isovector quark contributions cancel. It is possible that the inclusion of the  $f$ -quark excitation is necessary in this case, as suggested from our analysis of the inelastic scattering and helicity amplitudes.

## 7 Conclusions

While the results of our model for the scattering and electroproduction amplitudes in the case of the P11, P33 and S11 resonances provide good agreement with the experiment, in accordance with the limited scope of the rather simple underlying chiral quark model, the results for the  $D$ -wave resonances show a more pronounced disagreement, in particular for the prediction of the  $d$ -wave meson coupling to the quark core. The Cloudy Bag Model sharply cuts the quark wave-functions at the bag radius, and we cannot expect to be able to describe sufficiently well the peripheral region of the resonance to which the  $d$ -wave pions are sensitive; the same is true for the photon electric dipole and magnetic quadrupole interactions, which both involve  $l = 2$  photons. In order to reproduce the observed widths of the resonance it was therefore necessary to increase *ad hoc* the quark-model coupling constant by a factor of 1.4 in the case of the  $N(1520)$  and  $N(1700)$  and even by 2.4 in the case of the  $\Delta(1700)$  and  $N(1675)$ . Furthermore, the model predicts too small helicity amplitudes and consequently also the electroproduction amplitudes for the considered resonances. We have not tried to readjust the strength of the EM interaction to improve the agreement.

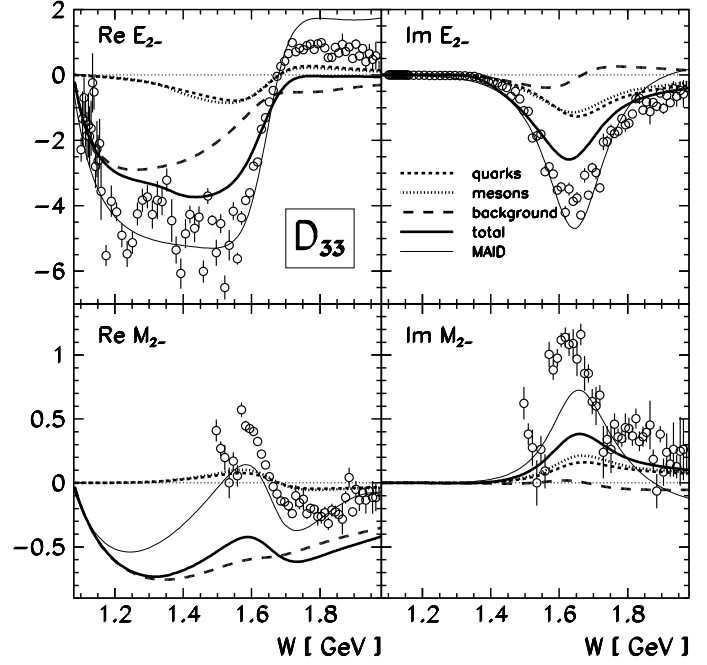


Fig. 9. The real and imaginary parts of the  $E_{2-}$  (top panels) and  $M_{2-}$  (bottom panels) electroproduction amplitudes in the D33 partial wave. Notation as in fig. 7.

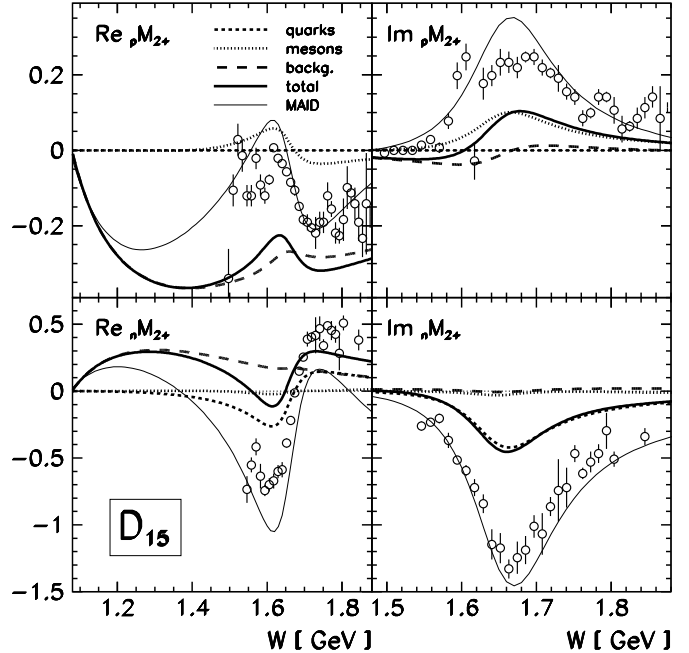


Fig. 10. The real and imaginary parts of the  $M_{2+}$  electroproduction amplitudes in the D15 partial wave, for the proton (top panels) and neutron targets (bottom panels). Notation as in fig. 7.

In order to get an insight into possible origins of the disagreement we have increased the bag radius and have been able to better reproduce the scattering amplitude in



the case of the D13 partial wave as well the  $M2$  (quadrupole) amplitude. This suggests that a better description of the peripheral part of the resonance wave-function is needed. The increase of radius, however, considerably spoils the inner part of the wave-function. Furthermore, our analysis of the scattering and helicity amplitudes indicates that the higher excitations (*i.e.* the  $f$ -state) of the quark core has to be included. Nonetheless, other quark model calculations using more sophisticated wave-functions obtain similar results for the helicity amplitude at least at small and modest  $Q^2$ . Our results, in particular for the D33 wave, show that the meson cloud effects are important in describing the long-range part of the wave-function and may eventually bring the results in the ballpark of acceptable values, which appear to be uncertain at the moment. In comparison with the P11 and P33 partial waves, which are dominated solely by  $p$ -wave mesons, the treatment of the meson cloud effects is much more sophisticated in the present case, where we encounter components of  $s$ -,  $p$ - and  $d$ -wave meson contributions of similar strengths. In fact, we have noticed a sizable cancellation of different contributions of the meson cloud, *e.g.* the vertex correction due to pion loops and the contribution from the direct coupling of the photon to the pion. It is therefore possible that in a more elaborate approach the meson-cloud effects would turn out to be stronger and would improve the agreement with experiment.

In spite of the deficiencies discussed above, we conclude that the overall qualitative agreement with the multipole analysis in the D13, D33 and D15 partial waves indicates that the quark-model explanation of the  $D$ -wave resonance as a  $p$ -wave excitation of the quark core, supplemented by the meson cloud, is sensible and that no further degrees of freedom are needed.

## A The weights for the unstable channels

The PV states (1) are normalized as

$$\langle \Psi^\alpha(W) | \Psi^\beta(W') \rangle = \delta(W - W') [\delta_{\alpha,\beta} + \mathbf{K}^2_{\alpha,\beta}]. \quad (16)$$

The PV states are not orthonormal; the orthonormalized states that enter the definition of the  $K$  matrix (2) are constructed by inverting the norm:

$$|\tilde{\Psi}^\alpha(W)\rangle = \sum_{\beta} [\mathbf{1} + \mathbf{K}^2]^{-1/2}_{\beta\alpha} |\Psi^\beta(W)\rangle. \quad (17)$$

We now explicitly construct the orthonormal states for the interesting region of energies close to a chosen resonance. Let us first note that in the vicinity of a resonance,  $\mathcal{R}$ , the PV state is dominated by the terms containing the pole, *i.e.* the quasi-bound quark state  $\Phi_{\mathcal{R}}$  and the corresponding component in the meson cloud (15):

$$|\Psi_{JT}^{MB}\rangle = \mathcal{N}_{MB} c_{\mathcal{R}}^{MB} |\hat{\Psi}_{\mathcal{R}}\rangle + \dots, \quad (18)$$

where ... stand for the non-resonant terms and

$$c_{\mathcal{R}}^{MB} = \frac{\mathcal{V}_{B\mathcal{R}}^M}{Z_{\mathcal{R}}(W)(W - M_{\mathcal{R}})}. \quad (19)$$

We introduce a shorthand notation

$$g_{MB} \equiv g_{\alpha} = \sqrt{\pi} \mathcal{N}_{MB} \mathcal{V}_{B\mathcal{R}}^M,$$

which, at the resonance, is just the square root of the half width  $\sqrt{\Gamma_{MB}/2}$  of the  $MB$  channel. Then

$$\begin{aligned} K_{\alpha\beta} &= \frac{g_{\alpha} g_{\beta}}{M_{\mathcal{R}} - W} + \dots \equiv (g_1^2 + g_2^2) \frac{r_{\alpha} r_{\beta}}{(M_{\mathcal{R}} - W)} + \dots \\ r_i &= \frac{g_i}{\sqrt{g_1^2 + g_2^2}}. \end{aligned} \quad (20)$$

For simplicity we restrict ourselves to the case of only two channels. The  $K$  matrix can be cast in the form

$$\mathbf{K} = \frac{(g_1^2 + g_2^2)}{(M_{\mathcal{R}} - W)} \begin{vmatrix} r_1 & -r_2 \\ r_2 & r_1 \end{vmatrix} \begin{vmatrix} 1 & 0 \\ 0 & 0 \end{vmatrix} \begin{vmatrix} r_1 & r_2 \\ -r_2 & r_1 \end{vmatrix} + \dots \quad (21)$$

*i.e.* the  $K$  matrix is proportional to the projector operator. It is then easy to derive the expression

$$\begin{aligned} (\mathbf{1} + \mathbf{K}^2)^{-\frac{1}{2}} &= \\ & \begin{vmatrix} r_1 & -r_2 \\ r_2 & r_1 \end{vmatrix} \begin{vmatrix} \frac{|M_{\mathcal{R}} - W|}{\sqrt{(M_{\mathcal{R}} - W)^2 + (g_1^2 + g_2^2)^2}} & 0 \\ 0 & 1 \end{vmatrix} \begin{vmatrix} r_1 & r_2 \\ -r_2 & r_1 \end{vmatrix} + \dots \\ &= \frac{|M_{\mathcal{R}} - W|}{\sqrt{(M_{\mathcal{R}} - W)^2 + (g_1^2 + g_2^2)^2}} \begin{vmatrix} r_1^2 & r_1 r_2 \\ r_1 r_2 & r_2^2 \end{vmatrix} \\ & \quad + \begin{vmatrix} r_2^2 & -r_1 r_2 \\ -r_1 r_2 & r_1^2 \end{vmatrix} + \dots \end{aligned} \quad (22)$$

From (3) and (19) it follows that close to the resonance the state on the RHS of (17) can be put in the form

$$|\Psi^\beta\rangle = \frac{K_{\alpha\beta}}{\sqrt{\pi} g_{\alpha}} |\hat{\Psi}_{\mathcal{R}}\rangle.$$

Evaluating the sum by using the expression (21) we notice that the second term in (22) vanishes

$$\begin{aligned} |\tilde{\Psi}^\alpha\rangle &= \sum_{\beta} (\mathbf{1} + \mathbf{K}^2)^{-\frac{1}{2}}_{\beta\alpha} |\Psi^\beta\rangle \\ &= \frac{g_{\alpha}}{\sqrt{\pi} \sqrt{(M_{\mathcal{R}} - W)^2 + (g_1^2 + g_2^2)^2}} |\hat{\Psi}_{\mathcal{R}}\rangle + \dots \\ &= \frac{1}{\sqrt{2\pi}} \frac{\sqrt{\Gamma_{MB}}}{\sqrt{(M_{\mathcal{R}} - W)^2 + \frac{1}{4}\Gamma^2}} |\hat{\Psi}_{\mathcal{R}}\rangle + \dots, \end{aligned} \quad (23)$$

where  $\Gamma = \sum_{M'B'} \Gamma_{M'B'}$ . The factor in front of the resonance state enters in the calculation of the  $K$ -matrix elements corresponding to the decay into this particular resonance,  $\mathcal{R}$ . In fact, only the square of the factor appears

$$w_{MB}(M) = \frac{1}{2\pi} \frac{\Gamma_{MB}(M)}{(M_{\mathcal{R}} - M)^2 + \frac{1}{4}\Gamma^2(M)},$$

where  $M$  is now used for the invariant mass of the  $MB$  system. The weights  $w_{MB}(M)$  are calculated in different partial waves and then stored using a spline approximation.

The result can be readily generalized to the case of three or more channels.

## B The $\rho qq$ and $\sigma qq$ vertices

The form of the  $\rho$ -meson coupling to the quarks in the Cloudy Bag Model has been discussed in [47]; they suggested a pion-like coupling at the bag surface. We therefore assume the Cloudy Bag Model type coupling

$$H_{\rho qq} = \frac{i}{2\tilde{f}_\rho} \int d\mathbf{r} \delta(r - R) \sum_t \psi^\dagger \boldsymbol{\alpha} \tau_t \psi \mathbf{A}_t. \quad (24)$$

Here  $\tilde{f}_\rho$  is analogous to  $f_\pi$  in the pion-quark interaction but there is no *a priori* reason to identify this parameter with the  $\rho$  decay constant,  $\tilde{f}_\rho \approx 200$  MeV.

In order to derive the form of the interaction for a particular partial wave it is most suitable to expand the  $\rho$  field in the basis with good total angular momentum  $J$ , its third component  $M$ , the orbital momentum  $l$ , and the third component of the isospin  $t$ :

$$\mathbf{A}_t = \sqrt{\frac{2}{\pi}} \int \frac{k dk}{\sqrt{2\omega_k}} \sum_{JlM} j_l(kr) \mathbf{Y}_{JlM}(\hat{\mathbf{r}}) a_{JlMt}(k) + \text{h.c.} \quad (25)$$

Here  $\mathbf{Y}_{JlM}(\hat{\mathbf{r}})$  are the vector spherical harmonics and  $a_{JlMt}(k)$  the meson annihilation operator. It is related to the corresponding operator of the plane-wave representation by

$$a_{JlMt}(k) = i^l k \int d\hat{\mathbf{k}} \sum_{\lambda m} Y_{lm}^*(\hat{\mathbf{k}}) C_{lm1\lambda}^{JM} a_{\lambda t}(\mathbf{k}), \quad (26)$$

where  $\lambda$  is the polarization ( $\lambda = 0, \pm 1$ ) and  $C_{lm1\lambda}^{JM}$  is the Clebsch-Gordan coefficient.

The  $N\rho$  channel can be labeled, in addition to specifying the total angular momentum  $J_{\text{ch}}$  and  $M_{\text{ch}}$ , by the relative angular momentum  $l$  and either by the spin  $S$  of the  $\rho N$  system or by the total angular momentum  $J_\rho$  of the  $\rho$ -meson. The two basis states are related through

$$|SlJ_{\text{ch}}M_{\text{ch}}\rangle = \sum_{J_\rho} \sqrt{2S+1} \sqrt{2J_\rho+1} W(lJ_{\text{ch}}1\frac{1}{2}; SJ_\rho) \times |J_\rho J_{\text{ch}} M_{\text{ch}} l\rangle, \quad (27)$$

where  $W(lJ_{\text{ch}}1\frac{1}{2}; SJ_\rho)$  is the Racah coefficient.

For the  $\rho qq$  interaction involving the  $s$ -state and the  $p_{j=1/2}$ -state quarks (SP) appearing in the negative parity partial wave we obtain

$$H_{\rho Jl}^{SP} = \int dk V_{Jl}^{\rho SP}(k) \sum_{i=1}^3 \sum_{Mt} \sigma_M(i) \tau_t(i) a_{lMt}(k) + \text{h.c.}, \quad (28)$$

with possible values  $J = 1$  and  $l = 0, 2$ :

$$V_{10}^{\rho SP}(k) = \frac{1}{4\pi\tilde{f}_\rho} \sqrt{\frac{\omega_{p_{1/2}}\omega_s}{(\omega_{p_{1/2}}+1)(\omega_s-1)}} \frac{2}{3} \frac{k^2}{\sqrt{\omega_k}} \frac{j_0(kR)}{kR},$$

$$V_{12}^{\rho SP}(k) = \frac{1}{4\pi\tilde{f}_\rho} \sqrt{\frac{\omega_{p_{1/2}}\omega_s}{(\omega_{p_{1/2}}+1)(\omega_s-1)}} \frac{\sqrt{2}}{3} \frac{k^2}{\sqrt{\omega_k}} \frac{j_2(kR)}{kR}.$$

Here  $\sigma_M$  acts between the total angular momenta of the quarks instead of their spins. For the  $\rho qq$  interaction between the  $s$ -state and the  $p_{j=3/2}$ -state quarks (SA) we find

$$H_{\rho Jl}^{SA} = V_{Jl}^{\rho SA}(k) \sum_{i=1}^3 \sum_{Mt} \Sigma_{JM}^{[\frac{3}{2}\frac{1}{2}]}(i) \tau_t(i) a_{JlMt}(k) + \text{h.c.} \quad (29)$$

with  $J = 1, l = 0, 2$  and  $J = 2, l = 2$ :

$$V_{10}^{\rho SA}(k) = \frac{1}{4\pi\tilde{f}_\rho} \sqrt{\frac{\omega_{p_{3/2}}\omega_s}{(\omega_{p_{3/2}}-2)(\omega_s-1)}} \frac{1}{\sqrt{3}} \frac{k^2}{\sqrt{\omega_k}} \frac{j_0(kR)}{kR},$$

$$V_{12}^{\rho SA}(k) = -\frac{1}{4\pi\tilde{f}_\rho} \sqrt{\frac{\omega_{p_{3/2}}\omega_s}{(\omega_{p_{3/2}}-2)(\omega_s-1)}} \frac{1}{\sqrt{6}} \frac{k^2}{\sqrt{\omega_k}} \frac{j_2(kR)}{kR},$$

$$V_{22}^{\rho SA}(k) = -\frac{1}{4\pi\tilde{f}_\rho} \sqrt{\frac{\omega_{p_{3/2}}\omega_s}{(\omega_{p_{3/2}}-2)(\omega_s-1)}} \sqrt{\frac{3}{2}} \frac{k^2}{\sqrt{\omega_k}} \frac{j_2(kR)}{kR},$$

where  $\langle \frac{3}{2} m_j | \Sigma_{JM}^{[\frac{3}{2}\frac{1}{2}]} | \frac{1}{2} m_s \rangle = C_{\frac{3}{2} m_s JM}^{\frac{3}{2} m_j}$ .

In the case of the interaction involving the  $s$ -state quarks alone, only the  $\rho$ -mesons with  $J = l = 1$  contribute, *i.e.* only the transverse magnetic M1 multipole is present:

$$H_{\rho qq} = \frac{1}{2\tilde{f}_\rho} \left( \frac{\omega_s}{\omega_s-1} \right) \frac{1}{2\pi} \sqrt{\frac{2}{3}} \int \frac{dk k^2}{\sqrt{\omega_k}} \frac{j_1(kR)}{kR} \times \sum_{i=1}^3 \sum_{tM} \sigma_M(i) \tau_t(i) [a_{11Mt}(k) + \text{h.c.}] \quad (30)$$

By using (26) this expression reduces to a more familiar form

$$H_{\rho qq} = \frac{i}{2\tilde{f}_\rho} \left( \frac{\omega_s}{\omega_s-1} \right) \frac{1}{3\sqrt{2\pi^3}} \int \frac{d\mathbf{k}}{\sqrt{2\omega_k}} \frac{3j_1(kR)}{kR} \times \sum_{i=1}^3 \sum_{t\lambda} \tau_t(i) (\boldsymbol{\sigma}(i) \times \mathbf{k}) \cdot \boldsymbol{\varepsilon}_\lambda a_{\lambda t}(\mathbf{k}) + \text{h.c.}, \quad (31)$$

which should be compared to the corresponding result in the pion case [38]

$$H_{\pi qq} = \frac{i}{2f_\pi} \left( \frac{\omega_S}{\omega_S-1} \right) \frac{1}{3\sqrt{2\pi^3}} \int \frac{d\mathbf{k}}{\sqrt{2\omega_k}} \frac{3j_1(kR)}{kR} \times \sum_{i=1}^3 \sum_t \tau_t(i) \boldsymbol{\sigma}(i) \cdot \mathbf{k} a_t(\mathbf{k}) + \text{h.c.} \quad (32)$$

We are now able to relate  $\tilde{f}_\rho$ , which determines the strength of the interaction in the Cloudy Bag Model, to the corresponding parameter in the pion case,  $f_\pi$ , in terms of the meson masses and the coupling constants  $f_{\pi NN}$  and  $f_{\rho NN}$ . In either case, relating the expectation value of the quark operators  $\sum_{i=1}^3 \tau(i)\sigma(i)$  in the nucleon to the corresponding operators acting on the nucleon isospin and spin, the same factor of  $5/3$  appears. Hence

$$\tilde{f}_\rho = \frac{m_\rho f_{\pi NN}}{m_\pi f_{\rho NN}} f_\pi.$$

Here  $f_{\rho NN}$  reads [25]

$$\frac{f_{\rho NN}}{m_\rho} = \frac{g_{\rho NN}(1 + k_\rho)}{4m_N}.$$

For typical values of  $g_{\rho NN}$  and  $k_\rho$  (see *e.g.* [25,20]) one obtains  $\tilde{f}_\rho \approx (1.5 \div 2) f_\pi$ .

For the weight function multiplying the  $\rho$ -meson vertices we assume a Breit-Wigner form modified by an energy-dependent correction involving the  $\rho$  range parameter [40].

As stressed in ref. [47], the number of  $\rho$  mesons is extremely small in the nucleon which means that the  $\rho$ -meson loops contribute little to the self energy and the vertex renormalizations. These contributions have therefore not been taken into account in our calculation.

The  $\sigma$ -quark interaction cannot be derived in an analogous way since it disappears at the bag surface. We therefore use a purely phenomenological approach as in [1]. For the  $s$ -wave we have assumed

$$V_0^\sigma(k, \mu) = V_0^\sigma(k) w_\sigma(\mu), \quad V_0^\sigma(k) = G_\sigma \frac{k}{\sqrt{2\omega_k}}.$$

Here  $\omega_k^2 = k^2 + \mu^2$ ,  $\mu$  is the invariant mass of the two-pion system and  $w_\sigma(\mu)$  is a Breit-Wigner weight function centered around  $m_\sigma = 450$  MeV with the width  $\Gamma_\sigma = 550$  MeV;  $G_\sigma$  is a free parameter determined in the  $N(1440)$  decay. For the  $p$ -wave we assume

$$V_{1m}^\sigma(k) = V_0^\sigma(k) \frac{kR}{3} \sum_{i=1}^3 \left[ \frac{1}{\sqrt{3}} \sigma_m(i) + \Sigma_{1m}^{\frac{3}{2}\frac{1}{2}}(i) \right],$$

where  $\sigma_m$  involves transition to the  $p_{\frac{1}{2}}$  quark state and  $\Sigma_{1m}^{\frac{3}{2}\frac{1}{2}}$  (defined above) to the  $p_{\frac{3}{2}}$  state.

## References

1. B. Golli and S. Širca, Eur. Phys. J. A **38**, 271 (2008).
2. B. Golli, S. Širca, and M. Fiolhais, Eur. Phys. J. A **42**, 185 (2009).
3. B. Golli, S. Širca, Eur. Phys. J. A **47**, 61 (2011).
4. M. Fiolhais, B. Golli, S. Širca, Phys. Lett. B **373**, 229 (1996).
5. I. G. Aznauryan and V. D. Burkert, Prog. Part. Nucl. Phys. **67**, 1 (2012).
6. I. G. Aznauryan et al., Int. J. Mod. Phys. E **22**, 1330015 (2013).
7. D. Drechsel, S. S. Kamalov, L. Tiator, Eur. Phys. J. A **34**, 69 (2007).
8. L. Tiator, D. Drechsel, S. S. Kamalov, M. Vanderhaeghen, Chinese Phys. C **33**, 1069 (2009).
9. L. Tiator, D. Drechsel, S. S. Kamalov, and M. Vanderhaeghen, Eur. Phys. J. Special Topics **198**, 141 (2011).
10. I. G. Aznauryan et al. (CLAS Collaboration), Phys. Rev. C **80**, 055203 (2009).
11. V. I. Mokeev, Phys. Rev. C **86**, 035203 (2012).
12. R. A. Arndt, W. J. Briscoe, I. I. Strakovsky, and R. L. Workman, Phys. Rev. C **74**, 045205 (2006).
13. [http://gwdac.phys.gwu.edu/analysis/pr\\_analysis.html](http://gwdac.phys.gwu.edu/analysis/pr_analysis.html).
14. A. V. Anisovich et al., Eur. Phys. J. A **48**, 15 (2012).
15. G. Penner and U. Mosel, Phys. Rev. C **66**, 055211 (2002).
16. M. Batinić, S. Ceci, A. Švarc, and B. Zauner, Phys. Rev. C **82**, 038203 (2010).
17. D. M. Manley, E. M. Saleski, Phys. Rev. D **45**, 4002 (1992).
18. M. Döring, Nucl. Phys. A **786**, 164 (2007).
19. M. Döring, E. Oset and D. Strottman, Phys. Lett. B **639**, 59 (2006).
20. D. Rönchen et al., Eur. Phys. J. A **49**, 44 (2013).
21. F. Huang et al., Phys. Rev. C **85**, 054003 (2012).
22. H. Kamano, S. X. Nakamura, T.-S. H. Lee, T. Sato, e-Print: [arXiv:1305.4351](https://arxiv.org/abs/1305.4351).
23. B. Juliá-Díaz et al., Phys. Rev. C **77**, 045205 (2008).
24. B. Juliá-Díaz et al., Phys. Rev. C **80**, 025207 (2009).
25. A. Matsuyama, T. Sato, T.-S. H. Lee, Physics Reports **439**, 193 (2007).
26. F. E. Close and F. J. Gilman, Phys. Lett. B **38**, 541 (1972).
27. M. Warns, H. Schröder, W. Pfeil, H. Rollnik, Z. Phys. C **46**, 627 (1990).
28. S. Capstick, B. D. Keister, Phys. Rev. D **51**, 3598 (1995).
29. M. Aiello, M. M. Giannini, E. Santopinto, J. Phys. G **24**, 753 (1998).
30. D. Merten, U. Löring, K. Kretzschmar, B. Metsch, H.-R. Petry, Eur. Phys. J. A **14**, 477 (2002).
31. E. Santopinto and M. M. Giannini, Phys. Rev. C **86**, 065202 (2012).
32. M. Ronniger and B. Ch. Metsch, Eur. Phys. J. A **49**, 8 (2013).
33. N. Isgur and G. Karl, Phys. Lett. B **72**, 109 (1977).
34. F. Myhrer and J. Wroldsen, Z. Phys. C **25**, 281 (1984).
35. T. A. deGrand, Ann. Phys. **101**, 496 (1976).
36. A. J. Hey et al., Nucl. Phys. A **362**, 317 (1981).
37. E. J. Garzon and E. Oset, Eur. Phys. J. A **48**, 5 (2012).
38. A. W. Thomas, Adv. Nucl. Phys. **13**, 1 (1984).
39. L. Tiator, D. Drechsel, G. Knoechlein, C. Bennhold, Phys. Rev. C **60**, 035210 (1999).
40. J. Beringer et al. (Particle Data Group), Phys. Rev. D **86**, 010001 (2012).
41. M. Dugger et al. (CLAS Collaboration), Phys. Rev. C **79**, 065206 (2009).
42. K. Joo et al., Phys. Rev. Lett. **88**, 122001 (2002).
43. G. Laveissiere et al., Phys. Rev. C **69**, 045202 (2004).
44. K. Park et al., Phys. Rev. C **77**, 015208 (2008).
45. G. Ramalho, M. T. Peña and F. Gross, Eur. Phys. A **36**, 329 (2008).
46. G. Ramalho and K. Tsushima, Phys. Rev. D **82**, 073007 (2010).
47. R. F. Alvarez-Estrada and A. W. Thomas, J. Phys. G: Nucl. Phys. **9**, 161 (1983).